Color Tuning of Nanofibers by Periodic Organic–Organic Hetero-Epitaxy

Clemens Simbrunner,[†,▽,*] Gerardo Hernandez-Sosa,[†,▽] Francesco Quochi,[‡,▽] Günther Schwabegger,[†] Chiara Botta,[§] Martin Oehzelt,[⊥] Ingo Salzmann,[¶] Tatjana Djuric,[#] Alfred Neuhold,[#] Roland Resel,[#] Michele Saba,[‡] Andrea Mura,[‡] Giovanni Bongiovanni,[‡] Antje Vollmer,[⊥] Norbert Koch,[¶] and Helmut Sitter[†]

[†]Institute of Semiconductor and Solid State Physics, Johannes Kepler University Linz, Austria, [‡]Dipartimento di Fisica, Università di Cagliari, SLACS-INFM/CNR, I-09042 Monserrato (CA), Italy, [§]Istituto per lo Studio delle Macromolecole, CNR, Via Bassini 15, I-20133 Milano, Italy, [⊥]Helmholtz Zentrum Berlin für Materialien und Energie GmbH, E-G1, Berlin, Germany, [¶]Institut für Physik, Humboldt-Universität zu Berlin, D-12489 Berlin, Germany, and [#]Institute of Solid State Physics, Graz University of Technology, Austria. [▽]These authors made substantially equivalent contributions.

ABSTRACT

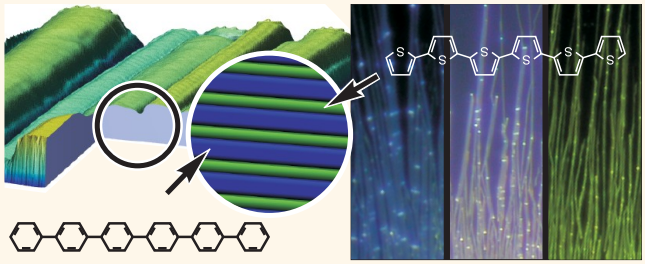

We report on the epitaxial growth of periodic para-hexaphenyl (*p*-6P)/α-sexi-thiophene (6T) multilayer heterostructures on top of *p*-6P nanotemplates. By the chosen approach, 6T molecules are forced to align parallel to the *p*-6P template molecules, which yields highly polarized photoluminescence (PL)-emission of both species. The PL spectra show that the fabricated multilayer structures provide optical emission from two different 6T phases, interfacial 6T molecules, and 3-dimensional crystallites. By a periodical deposition of 6T monolayers and *p*-6P spacers it is demonstrated that the strongly polarized spectral contribution of interfacial 6T can be precisely controlled and amplified. By analyzing the PL emission of both 6T phases as a function of *p*-6P spacer thickness (Δd_{p-6P}) we have determined a critical value of $\Delta d_{p-6P} \approx 2.73$ nm where interfacial 6T runs into saturation and the surplus of 6T starts to cluster in 3-dimensional crystallites. These results are further substantiated by UPS and XRD measurements. Moreover, it is demonstrated by morphological investigations, provided by scanning force microscopy and fluorescence microscopy, that periodical deposition of 6T and *p*-6P leads to a significant improvement of homogeneity in PL-emission and morphology of nanofibers. Photoluminescence excitation experiments in combination with time-resolved photoluminescence demonstrate that the spectral emission of the organic multilayer nanofibers is dominated by a resonant energy transfer from *p*-6P host- to 6T guest-molecules. The sensitization time of the 6T emission in the 6T/*p*-6P multilayer structures depends on the *p*-6P spacer thickness, and can be explained by well separated layers of host–guest molecules obtained by organic–organic heteroepitaxy. The spectral emission and consequently the fluorescent color of the nanofibers can be efficiently tuned from the blue *via* white to the yellow-green spectral range.

KEYWORDS: para-hexaphenyl · sexi-thiophene · organic–organic heteroepitaxy

During the past few years, a strong scientific focus could be recognized concerning the self-assembly of highly ordered nanostructures, based on nanocrystals[1,2] or inorganic and organic building blocks.[3−6] The ability to assimilate the advanced functions and properties into numerous applications[7] motivates the study of self-assembled nanostructures providing a proper foundation for the realization of functional materials and devices.

A lot of effort has been invested in the past to understand the epitaxial growth of organic nanofibers on muscovite mica substrates.[8−12] It turned out that among the huge class of available molecules which tend to crystallize in the shape of organic-nanofibers on mica substrates, para-phenylenes are outstanding in this quality.[8,13] Along with robustness against chemicals or heat treatment,[14] the ability of para-hexaphenyl (*p*-6P) to form highly parallel aligned nanofibers consisting of parallel oriented molecules, motivated detailed growth studies. Thus, the high potential for optoelectronic devices has been evidenced due to the demonstration of waveguiding[15,16] and lasing.[17−19]

On the contrary, the attempt to substitute *p*-6P by thiophenes or thiophene/phenylene co-oligomers to tune photoluminescence (PL)-emission properties from the blue to the green and red spectral range ended up in much lower morphological and optical anisotropy.[9,20] Until now, parallel molecular alignment on muscovite mica and thus macroscopic polarized emission has only been demonstrated for a small group of molecules[21] and can be explained by an outstanding molecular adsorption geometry[8] of phenylenes relative to the muscovite mica substrate. This phenomenon further underlines that a substitution of *p*-6P by other molecular species represents a demanding challenge for the fabrication of self-assembled nanofibers. To summarize, more complex approaches have to be found to achieve efficient tuning of the nanofibers' optical properties in combination with a conserved polarized emission.[22,23]

* Address correspondence to clemens.simbrunner@jku.at.

Received for review May 6, 2011 and accepted May 17, 2012.

Published online May 17, 2012
10.1021/nn2047235

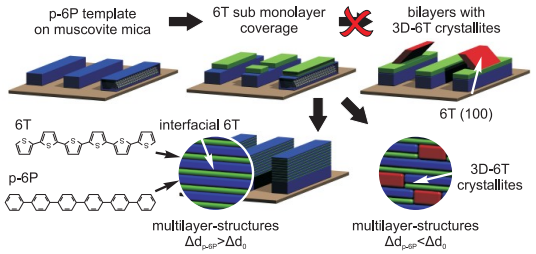

Figure 1. Graphical summary of *p*-6P/6T nanofiber growth. After deposition of *p*-6P, deep blue emitting nanofibers are obtained. The overgrowth of these templates by 6T molecules with nominally submonolayer coverage leads to green fluorescence. Further deposition of 6T leads to the formation of 3D-6T crystallites which emit in the orange/red spectral range. These crystallites are characterized by clusters on top of the fiber templates, which provide a significant tilt of their (100) low index plane. As indicated below, an alternating deposition of 6T/*p*-6P leads to an inforced formation of green emitting interfacial 6T. If inserted, *p*-6P spacers obtain a thickness ($\Delta d_{p\text{-}6P}$) above the critical value (Δd_0) nucleation of 3D-6T crystallites is suppressed, whereas for samples with $\Delta d_{p\text{-}6P} < \Delta d_0$ the formation of 3D-6T crystallites is observed.

It has been demonstrated that organic−organic heteroepitaxy of nanofibers can provide a proper method to influence the molecular alignment in a positive and controlled way.[24,25] In particular, it has been shown that sexi-thiophene (6T) molecules, which have been deposited by hot wall epitaxy (HWE) on top of *p*-6P nanofiber templates adopt the specified nano- and macroscopic order leading to highly polarized emission in the green and red spectral range.[23] Intense green fluorescence has been observed for nanofibers with nominally submonolayer (ML) coverage of 6T, whereas red emission could be attributed to 3-dimensional (3D)-6T crystallites which have nucleated on top of the *p*-6P templates when the 6T coverage is increased (sketched in the first row of Figure 1). It has been observed that the PL-emission intensity of 3D-6T crystallites under UV excitation is much weaker than the green emission of interfacial 6T molecules, which can be explained by an effective sensitization by *p*-6P molecules *via* energy transfer.[23] Additionally, it has been demonstrated that nanofibers, which provide a low 6T coverage, are characterized by a homogeneous morphology and optical emission properties, whereas red emitting 3D-6T crystallites tend to form clusters on top of the *p*-6P template. Moreover, transmission electron microscopy analysis of bilayer *p*-6P/6T nanofibers' revealed that cross sections of *p*-6P and 6T crystallites significantly differ. Whereas *p*-6P nanofibers are characterized by a quasi-rectangular shape, 6T crystallites which have nucleated on top are remarkablely tilted due to the configuration of their (100) low index plane.[23] The size and shape of the fiber cross sections play a significant role for a successful implementation of lasing as an optical feedback along the nanofibers' axes, which can only be provided if the light is waveguided within the nanofiber.[15,17,26] As indicated by the sketch in Figure 1 the tilt angle of 6T crystallites entails a smaller cross-sectional area, which, in combination with self-absorption processes, may reduce effective waveguiding. All these observations motivate the effort to force a predominant formation of green emitting 6T ML, which seems advantageous for the fabrication of opto-electronic devices. Obviously the proposed goal coincides with the concept of an increased number of *p*-6P/6T interfaces.

RESULTS AND DISCUSSION

To analyze the influence of periodical deposition of *p*-6P/6T on top of *p*-6P nanofiber templates we have used a growth chamber which has been equipped with a HWE reactor for *p*-6P and a separate one for 6T evaporation. To ensure stable growth conditions the muscovite mica substrates, which have been freshly cleaved in air, are continuously heated to 120 °C.[23] In a first step, a *p*-6P template layer has been evaporated with a nominal thickness of ∼33 nm. Subsequently, the sample is periodically transferred between 6T and *p*-6P HWE reactors in high vacuum conditions. During each deposition cycle a ML coverage ($\Delta d_{6T} \approx 0.38$ nm) of 6T molecules has been inserted, which is subsequently buried by a *p*-6P spacing layer. Consequently, the number of deposition cycles (n) is representative of the number of 6T monolayers, which are sandwiched between *p*-6P spacers.

To study the influence of the *p*-6P spacing layer thickness ($\Delta d_{p\text{-}6P}$) on the fluorescence emission, a sample series (i) has been fabricated where the number of 6T layers has been kept constant ($n = 10$), but the *p*-6P spacer thickness ($\Delta d_{p\text{-}6P}$) has been continuously increased from 16 nm up to 325 nm (a graphical sketch of the sample preparation is depicted in Figure 2a). By the chosen growth conditions all nanofibers contain the same amount of 6T molecules, whereas the amount of *p*-6P is continuously increased. In that way the total thickness of the periodically deposited layer sequence exhibits at least 160 nm. Consequently, we can assume that the influence of the *p*-6P template layer on the nanofibers' optical response in photoluminescence (PL) can be neglected and a relative reduction of the 6T PL intensity compared to the *p*-6P PL can be expected with increasing $\Delta d_{p\text{-}6P}$.

In a first step PL was chosen to characterize the fabricated nanofibers. As indicated in Figure 2b, all samples are characterized by two well separated emission bands, which can be attributed to *p*-6P (350−500 nm) and 6T (500−700 nm).[23] To provide a direct comparison between the 6T PL emission intensity and growth parameters, emission spectra have been normalized to the *p*-6P (0−1) peak. For a detailed analysis, spectral emissions have been decomposed into 3D and interfacial 6T contributions.[23] (see Supporting Information) Within the discussed samples series all emission spectra are dominated by blue

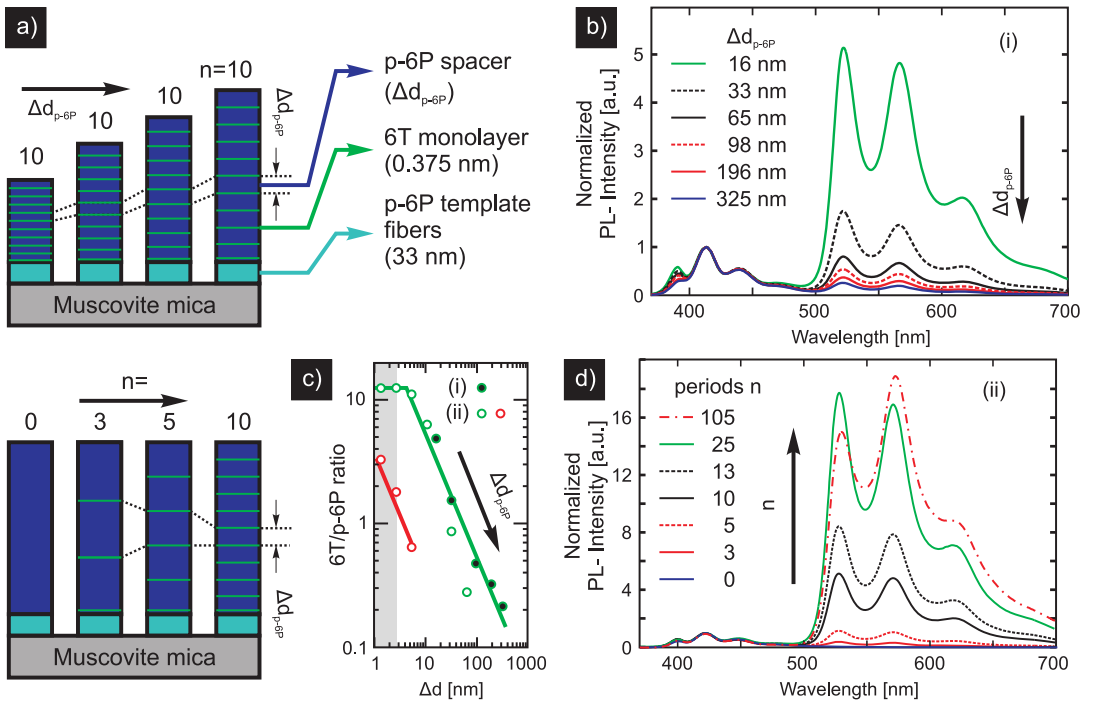

Figure 2. (a) Graphical sketch of the sample geometries. For the fabrication of series I a constant number of 6T monolayers (n = 10) has been chosen, whereas p-6P spacer thickness ($\Delta d_{p\text{-}6P}$) has been varied (top panel). For series ii the total amount of p-6P has been kept constant, whereas the number of 6T interfaces has been gradually increased (lower panel). (b) Fluorescence spectra of periodically grown p-6P/6T nanofibers of series I normalized to p-6P (0−1) emission. All spectra are characterized by p-6P and interfacial 6T contributions and no contributions of crystalline 6T can be dedected. (c) Spectral contributions of interfacial (green circles) and bulk 6T (red circles) as a function of $\Delta d_{p\text{-}6P}$. Open/solid circles indicate data points deduced from series i/ii. Solid lines indicate linear fits to the data. (d) Normalized fluorescence spectra of series ii. With increasing number of 6T layers green emission is significantly inforced. For samples with more than n = 50 periods ($\Delta d_{p\text{-}6P} \leq$ 2.73 nm) also contributions of 3D-6T crystallites are observed (red dashed-dotted spectrum).

p-6P and green interfacial 6T emissions and no contributions of crystalline 3D-6T could be detected, which underlines that the formation of red emitting 6T crystallites has been successfully suppressed. On the basis of this analysis, the resulting, weighting factors for the green emitting interfacial 6T phase (($I_{max,6T}$)/-($I_{max,p\text{-}6P}$)) are plotted by black filled circles in Figure 2c as a function of $\Delta d_{p\text{-}6P}$. As indicated by a solid green line, the interfacial 6T emission linearly decreases with increasing $\Delta d_{p\text{-}6P}$ which indicates that the ratio of the emission intensities of p-6P and 6T is proportional to the overall concentration of 6T, which can be approximated by $\Delta d_{6T}/\Delta d_{p\text{-}6P}$ for $\Delta d_{p\text{-}6P} \gg \Delta d_{6T}$.

In a second step, a series (ii) of samples were prepared where the number of inserted 6T layers (n = 3, 5, 10, 13, 25, 50, 105) was varied. To keep the total thickness of the nanofibers constant (∼175 nm for all fabricated samples) the p-6P spacer thickness was accordingly decreased (∼65, ..., 5.5, 2.73, 1.36 nm) with increasing number of 6T/p-6P deposition cycles (a graphical sketch of the growth conditions is depicted in the lower part of Figure 2a). For the deposition of 6T during each period, we have again chosen a ML coverage (∼0.38 nm) of 6T molecules. Consequently, the total amount of p-6P has been kept constant within the whole series ii, whereas the nominal 6T concentration increases proportional to the number of deposition cycles n. The discussed growth conditions were chosen for two main reasons. On the one hand the number of deposition cycles n has to be increased for small $\Delta d_{p\text{-}6P}$ to ensure that the spectral contribution of the p-6P template layer can be neglected. On the other hand it should be demonstrated that the number of deposition cycles plays a minor role for the nanofibers' spectral emission, whereas $\Delta d_{p\text{-}6P}$ represents the key parameter to tune the spectral contribution of 6T.

Again, PL spectra have been acquired and are presented in 2d normalized to p-6P (0−1) emission. Obviously, the relative intensity of the 6T emission is continuously increasing, with increasing number of growth cycles n, and consequently raising 6T concentration. Down to a p-6P spacer thickness of ∼5.5 nm (n = 25, green line) no saturation effects are observed, and only green emitting interfacial 6T phase is dominantly detected. Again, this underlines the successful suppression of 3D-6T crystallites at the discussed growth conditions. At higher periodicities (n = 50, 105) and consequently for nanofibers with smaller p-6P spacer layers $\Delta d_{p\text{-}6P} \leq d_0$ = 2.73 nm, the increase of interfacial 6T emission runs into saturation and a clear contribution in the red spectral range, originating from 3D-6T crystallites, is observed in the spectra (see Figure 2d, red dashed-dotted line).

To compare the fluorescence of both sample series, spectral emissions have been decomposed into 3D and interfacial 6T contributions[23] and the resulting weighting factors are plotted by open green (interfacial) and red (3D crystal) circles in Figure 2c as a function of $\Delta d_{p\text{-}6P}$. Interfacial 6T contributions not only follow a linear behavior but also overlap with experimental results obtained for sample series I, which underlines that $\Delta d_{p\text{-}6P}$ represents the key parameter to tune nanofibers' emission. Moreover, a gray area indicates the critical *p*-6P spacer thickness of approximately ($\leq$2.73 nm), where the PL intensity of the green emitting 6T phase runs into saturation and concurrently a significant contribution of 3D-6T emission is observed. It is worth noting that also the PL intensity of bulk 6T linearly decreases with increasing $\Delta d_{p\text{-}6P}$ as indicated by a red solid line in Figure 2c.

On the basis of PL analysis, it can be concluded that periodical deposition of *p*-6P/6T layers on nanofibers' templates can be used to precisely control and amplify the interfacial green emission of 6T. Nevertheless, there exists a critical thickness of the *p*-6P spacer ($\Delta d_0 \approx 2.73$ nm) which is necessary to avoid the nucleation of 6T crystallites (summarized in Figure 1). As the nucleation of 6T crystallites coincides with a saturation of interfacial 6T emission, this critical $\Delta d_{p\text{-}6P}$ also defines the growth conditions where interfacial 6T emission yields its maximum spectral contribution.

To prove the drawn picture and in particular to study the formation of the *p*-6P/6T interface in detail, surface sensitive methods such as ultraviolet photoelectron spectroscopy (UPS) were carried out.[27,28] Muscovite mica is well-known for its excellent thermal and electrical isolation, which represents a serious drawback for UPS analysis due to charging effects. Preliminary growth studies using highly ordered pyrolytic graphite (HOPG) as substrate have shown that *p*-6P nucleates in the same crystal phase and contact plane as observed for mica. Only the azimuthal orientation of *p*-6P crystallites is significantly different on both substrates, which plays a minor role for the formation of the *p*-6P/6T/*p*-6P interface. Consequently, *p*-6P has been deposited on a HOPG substrate using molecular beam epitaxy (MBE) yielding a nominal layer thickness of 5 nm. Subsequently UPS spectra have been recorded with a takeoff angle of 45°. The resulting UPS spectrum is depicted in Figure 3a showing a double peak structure (the positions are indicated by blue dotted lines) between 2 and 3 eV binding energy, which is representative for flat lying *p*-6P molecules.[28] In a further step 0.4 nm of 6T (corresponding to approximately one monolayer coverage) was deposited on top of the *p*-6P template layer. Strikingly, it can be observed that the characteristic *p*-6P peak located at higher binding energies efficiently quenches, whereas an additional peak arises at about 1.5 eV. The fact that the peak, which is located around 2 eV, shows a quasi-static behavior can

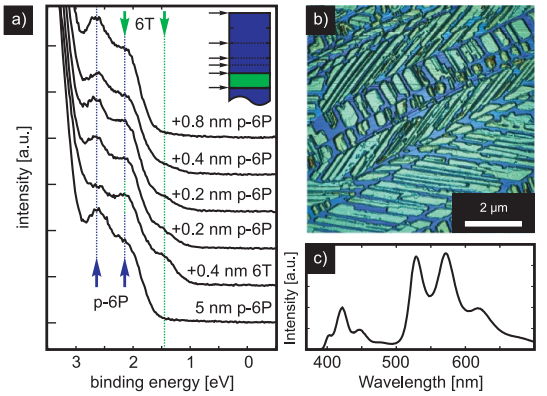

Figure 3. (a) Ultraviolet photoemission spectroscopy (UPS) data obtained on a *p*-6P/6T/*p*-6P heterostructure deposited on HOPG. Black arrows in the inset indicate the nominal layer thickness where UPS spectra have been acquired. Green (blue) lines indicate HOMO, HOMO-1 positions of 6T (*p*-6P). (b) Scanning force microscopy image of the fabricated structure showing a homogeneous height distribution yielding a coverage of approximately 70% of the samples surface. (c) PL spectrum of the *p*-6P/6T/*p*-6P heterostructure deposited on HOPG.

be explained by the coincidence that the highest organic molecular orbital (HOMO) of *p*-6P and the HOMO-1 of 6T appear at the same binding energy. Peak positions, which are representative for the HOMO and HOMO-1 of 6T, are indicated by green dotted lines. On the basis of these results it can be concluded that 6T molecules form a quasi-closed layer after the deposition of 1 ML, which further substantiates the highly homogeneous green fluorescence of *p*-6P nanofibers.[23]

To investigate the *p*-6P/6T/*p*-6P interface formation in more detail, 0.2 nm of *p*-6P was deposited on top of the 6T ML. The resulting spectrum, which is demonstrated in Figure 3a, is characterized by a significant increase of the *p*-6P HOMO-1 peak accompanied by a quenching of 6T HOMO due to a *p*-6P layer formation on top of the organic template. Nevertheless, a clear fingerprint of 6T molecules at the surface is still present. Consequently, *p*-6P deposition was resumed and was interrupted for acquiring UPS spectra after 0.4, 0.8, and 1.6 nm of nominal *p*-6P coverage on top of the 6T ML (a graphical sketch is depicted in the inset of Figure 3a). As indicated in Figure 3a the 6T HOMO peak continuously quenches with increasing *p*-6P coverage and finally disappears for a *p*-6P coverage of about 1.6 nm. Consequently, the drawn picture, which has been deduced by PL analysis on nanofibers grown on muscovite mica, can be further substantiated. In particular the formation of 6T crystallites for relative small *p*-6P spacing layers ($\leq$2.73 nm) can be understood by the fact that *p*-6P molecules do not cover the whole fiber surface, which leads to an increased probability for 3D-6T nucleation. The deduced picture is further underlined by X-ray diffraction (XRD) measurements indicating the presence of 6T,

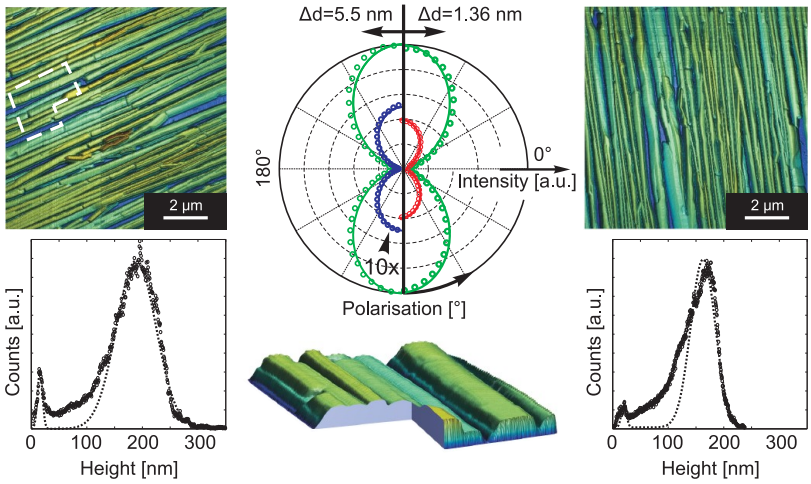

Figure 4. (center) Polarization-dependent emission of *p*-6P (blue, 10× magnified), interfacial (green), and bulk 6T components (red) for samples of series ii grown on muscovite mica with $\Delta d_{p\text{-}6P}$ = 5.5 nm (left) and $\Delta d_{p\text{-}6P}$ = 1.36 nm (right). Data has been normalized to interfacial 6T emission and solid lines indicate $\cos^2$ fits to the data. SFM images and height distributions for periodically grown nanofibers with $\Delta d_{p\text{-}6P}$ = 5.5 nm (left) and $\Delta d_{p\text{-}6P}$ = 1.36 nm (right) are depicted. All nanostructures show a highly homogeneous height distribution. The bottom part of the figure indicates a cross-sectional view of the area marked by a dashed polygon in the corresponding SFM image (top, left).

which crystallizes in the low temperature (LT) phase[29] for nanofibers fabricated under such conditions on muscovite mica (see Supporting Information for details). The fact that no significant energetic shift of HOMO levels can be observed neither for *p*-6P nor 6T further underlines the picture that 6T molecules are sandwiched in between *p*-6P spacing layers and do not form a mixed crystal phase as, for example, observed for coevaporation of *p*-6P/6T.[30,31] It has to be stated that these findings are also in agreement with XRD results, which hint at the sole presence of the *p*-6P β-phase[32] and 6T LT phase[29] in periodically deposited *p*-6P/6T nanofibers.

After the fabrication of the *p*-6P/6T/*p*-6P heterostructure the sample was exposed to air, and the surface morphology was studied by scanning force microscopy (SFM). As indicated by the SFM image shown in Figure 3b the sample surface is characterized by two height levels which can be attributed to the bare HOPG substrate and organic crystallites. It can be clearly seen that the organic film is not completely closed but forms nanostructures covering approximetly 70% of the substrates surface which is essential to be able to infer UPS results to nanofibers fabricated on muscovite mica. To demonstrate that also optical response behaves in an analogous way, PL experiments were carried out and results are presented in Figure 3c. It can be clearly seen that the spectral emission is dominated by two emission centers which can be attributed to *p*-6P and green emitting interfacial 6T phase. On the basis of these results, it can be stated that UPS, XRD, and PL analysis leads to a consistent picture concerning the formation of the organic−organic interface.

In a next step SFM and polarization-dependent optical spectroscopy has been applied to investigate the nanofibers' morphology and the relative molecular alignment between *p*-6P and 6T within the nanofibers, again grown on muscovite mica, in more detail. Two representative samples were chosen and spectral contributions of interfacial-6T (green), bulk-6T (red) and *p*-6P (blue) emissions are presented as a function of polarization angle by means of a polar plot in the center of Figure 4. Both data sets are normalized to the interfacial green emission. In a first step the orientation of interfacial 6T relative to *p*-6P molecules is analyzed ($\Delta d_{p\text{-}6P}$ = 5.5 nm) in the left part of the polar plot. Because of the strong quenching of blue *p*-6P emission, its spectral contribution has been magnified by a factor of 10. Obviously, both molecular species are characterized by high anisotropy and provide a congruent shape of their emission characteristics. Solid lines indicate $\cos^2$ fits to the data quantifying parallel molecular orientation and intensity ratios on the order of 10.97 (11.8) for *p*-6P and 6T emission, respectively. Analogous values 10.58/12.64 for *p*-6P/6T are obtained for samples which contain 3D-6T crystallites ($\Delta d_{p\text{-}6P}$ = 1.36 nm). To increase readability only contributions of interfacial and bulk 6T emissions are presented in the corresponding polar plot (right part). Again, congruence of the bar-bell shaped $\cos^2$ fits underlines a highly parallel alignment of 6T molecules for both phases. Nevertheless, intensity ratios on the order of 7.5 hint a slightly lower anisotropy for 3D-6T crystallites which could be caused by a molecular realignment during crystallization[8,10] to provide an optimized lattice match. On the basis of the polarization dependent optics combined with XRD pole figure measurements (see Supporting Information) we conclude that 3D-6T emissions originate from 6T crystals which have nucleated on *p*-6P nanofibers in the low-temperature phase.[29] Concerning the geometrical alignment of 6T crystallites, it can be stated that they provide the same

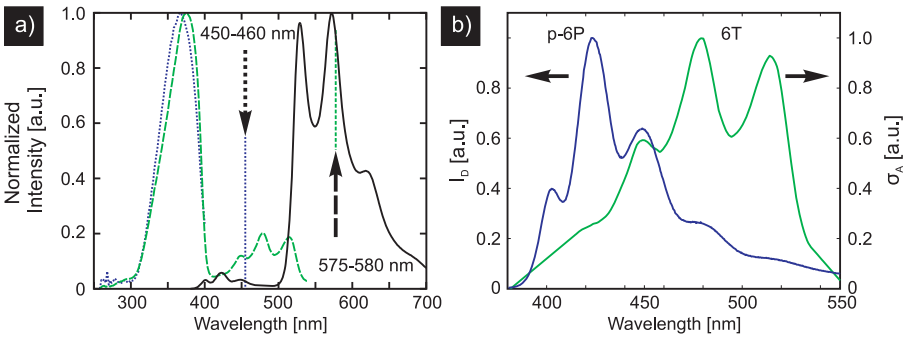

Figure 5. (a) Photoluminescence spectrum of periodically grown *p*-6P/6T sample with $\Delta d_{p\text{-}6P}$ = 2.73 nm, excited at 325 nm continuous-wave (black line); photoluminescence excitation spectra detected in the 450−460 nm and 575−580 nm bands (green dashed and blue dotted line, respectively). Central wavelengths of detection bandwidths are indicated by the dashed arrows. (b) Normalized emission spectrum of *p*-6P (blue line) and absorption spectrum of 6T (green line).

contact plane ($\bar{4}11$) and azimuthal alignment as already reported for *p*-6P/6T bilayer nanofibers, which is also consistent with polarization dependent PL measurements.[23]

Concerning sample morphology it can be stated that all fabricated samples show highly parallel aligned nanofibers (see Supporting Information). Exemplarily, SFM images of those samples have been selected which have been investigated by polarization dependent optics and are depicted on the left and right sides in Figure 4. Whereas no significant contributions of 6T crystallites could be detected in the nanofibers shown on the left side ($\Delta d_{p\text{-}6P}$ = 5.5 nm), PL emission of nanofibers presented on the right side of Figure 4 clearly showed contributions of 3D-6T emission. Nevertheless, height distributions of both samples are dominated by only two height levels which can be attributed to the muscovite mica substrate and the mean height of the nanostructures. Consequently, the needle morphology, which is characteristic for *p*-6P nanofibers on muscovite mica, could be conserved, whereas the formation and nucleation of 6T crystallites[23] on top of the template fibers is suppressed. As indicated by a cross-sectional view (the corresponding area is indicated by a white polygon in the SFM image) in the bottom of Figure 4 all nanofibers are characterized by a quasi-rectangular shape which further approves the presented growth procedure in order to tune nanofibers' emission but prevent the formation of significantly tilted and narrow 6T crystallites on top of *p*-6P fiber templates.

Photoluminescence excitation (PLE) spectroscopy gives valuable information on the 6T absorption lineshapes and allows for practical demonstration of 6T emission sensitization *via* energy transfer upon *p*-6P optical excitation. Measurements are done in a 6T-rich sample (9.25% relative concentration, $\Delta d_{p\text{-}6P}$ = 2.73 nm) for best sensitivity to 6T absorption. Experimental results are shown in Figure 5. The PLE spectrum taken with 450−460 nm detection bandwidth hints to a *p*-6P optical absorption resonance peaked at ~370 nm. When the detection bandwidth is moved to 575−580 nm, where only 6T emits, the PLE spectrum shows a multipeak structure extending between 400 and 550 nm, which is ascribed to 6T vibronic absorption, whereas a nearly identical resonance peak is reported below 400 nm. Photoexcited *p*-6P is thus understood to sensitize the 6T emission in the multilayered sample structure by nonradiative (Förster's) energy transfer. The critical radius of energy transfer (or Förster's radius, R_0) can be estimated based on the knowledge of donor/acceptor dipole orientations and the spectral overlap between the donor optical emission and the acceptor optical absorption. Förster's radius is calculated as

$$R_0 = \sqrt[6]{\frac{9k^2 J Q_D}{128\pi^5 n^4}} \quad (1)$$

where $J = \int I_D(\lambda)\sigma_A(\lambda)\lambda^4 \, d\lambda$ is the overlap integral between the normalized donor emission spectrum I_D and the acceptor absorption cross-section spectrum σ_A, and Q_D is the donor emission quantum yield in the absence of the acceptor. The orientational factor, k^2, is calculated for parallel donor/acceptor transition dipoles upon averaging over an isotropic positional distribution of dipoles (k^2 = 0.8). The PLE multipeak structure extending between 400 and 550 nm is assumed to yield the acceptor absorption line shape [see Figure 5b]. Given a peak value of 1.8×10^{-16} cm^2 for the 6T absorption cross-section as for 6T in solution[33] and further assuming Q_D = 0.3,[34] eq 1 yields R_0 = 3.6 nm.

The energy transfer dynamics is investigated by time resolving the *p*-6P and 6T optical emissions upon sample excitation by ultrashort pulses tuned to the *p*-6P absorption peak. Time traces of 6T emission as a function of *p*-6P spacer thickness are reported in Figure 6a. Traces are best reproduced by the sum of two contributions, that is, a prompt emission signal, which starts at the very instant of laser pulse excitation, and a delayed emission signal reaching its maximum tens to hundreds of picoseconds after pulsed excitation

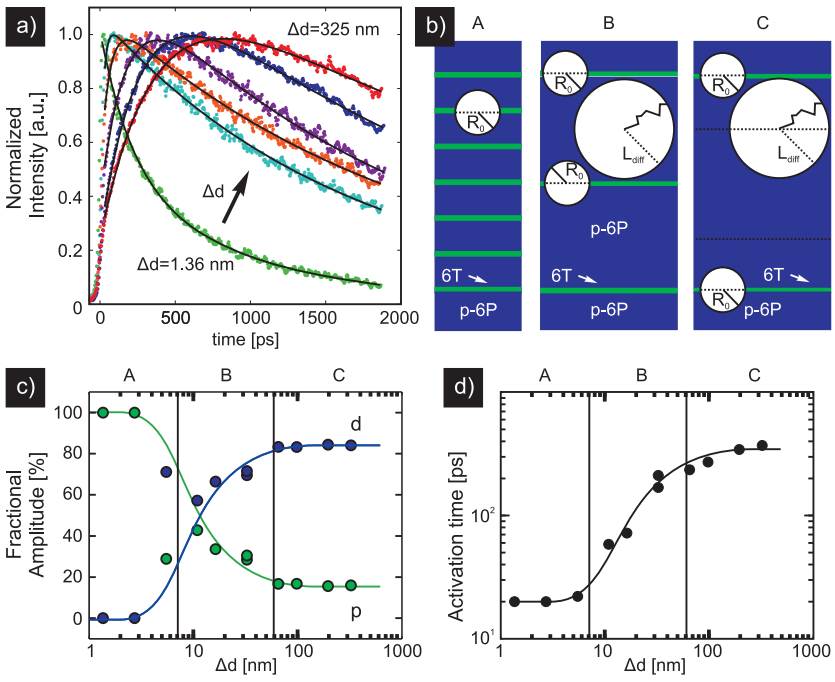

Figure 6. (a) Time traces of 6T emission intensity of periodically grown *p*-6P/6T nanofibers excited by 150 ps laser pulses at 378 nm central wavelength as a function of *p*-6P spacer thickness ($\Delta d_{p\text{-}6P}$). The emission intensity is integrated over the 550−610 nm wavelength interval. Dots, experimental data; lines, fit curves; see text for details. (b) Schematic representation of Förster's sphere and diffusion sphere in three different regimes for $\Delta d_{p\text{-}6P} < 2R_0$ (A); $2R_0 < \Delta d_{p\text{-}6P} < 2L$ (B); $\Delta d_{p\text{-}6P} > 2L$ (C). (c) Fractional amplitudes of prompt (p) and delayed (d) components of 6T emission dynamics *versus* $\Delta d_{p\text{-}6P}$; vertical lines correspond to $\Delta d_{p\text{-}6P} = 2R_0$ (left) and $\Delta d_{p\text{-}6P} = 2L$ (right). (d) Activation time of 6T emission *versus* $\Delta d_{p\text{-}6P}$. Vertical lines are the same as in panel c. Continuous lines in panels c and d are guides for the eye.

and then decaying in the nanosecond time scale (see *p*-6P decay dynamics and time-wavelength spectrogram of *p*-6P and 6T emissons in the Supporting Information). Given that prompt and delayed emission transients refer to the same type of 6T excitations, the two signal components should decay with the same time constant. In a simple phenomenological approach, the time profiles of the 6T emission can be fitted with the function

$$I_{6T}(t) = A_P e^{-t/\tau_{dec}} + A_d(1 - e^{-t/\tau_{act}+t/\tau_{dec}})e^{-t/\tau_{dec}} \quad (2)$$

where A_P is the amplitude of the prompt emission component, A_d is the amplitude of delayed emission component, τ_{act} is the activation time of the 6T delayed emission, and τ_{dec} is the 6T emission decay time. The signal fractional amplitudes, $A_p/(A_p+A_d)$ and $A_d/(A_p+A_d)$, and τ_{act} are shown as a function of *p*-6P spacer thickness in Figure 6c and 6d, respectively. For small spacer thicknesses, 6T emission is dominated by the prompt component, and signal rise time is limited by the instrumental resolution (~20 ps). For $\Delta d_{p\text{-}6P}$ exceeding ~4 nm, the delayed component progressively gains strength at the prompt component expenses and activation time increases with growing $\Delta d_{p\text{-}6P}$. In the large thickness limit ($\Delta d_{p\text{-}6P} > 60$ nm), sensitization dynamics become fairly insensitive to spacer thickess. The prompt component of the 6T emission transient is ascribed to direct, or single-step energy transfer between donor−acceptor molecules placed at distances shorter than R_0. This attribution is supported by the observation that the delayed emission component vanishes for $\Delta d_{p\text{-}6P} < 2R_0 \approx 7$ nm, where all donor excitations fall within Förster's distance from the nearest 6T layer and 6T sensitization dynamics is virtually faster than the response time of our experimental apparatus. The delayed emission component is in turn attributed to energy transfer events mediated by exciton diffusion within the photoexcited *p*-6P spacing layers. In organic epitaxial films exciton diffusion length (L) can be as large as tens of nanometers, a length scale that is comparable to that of crystal grain size.[35] Donor excitations created in a given *p*-6P spacer at a distance from nearest 6T layer larger than L should not contribute to 6T sensitization, and thus for $\Delta d_{p\text{-}6P} > 2$ L sensitization dynamics should be practically insensitive to spacer thickness. Since this occurs for $\Delta d_{p\text{-}6P} > 60$ nm, exciton diffusion length in *p*-6P spacers is estimated to be ~30 nm. The results shown in Figure 6c,d are fairly insensitive to variations of pump laser penetration depth, which can be increased upon tuning the pump wavelength close to the *p*-6P optical absorption edge near 405 nm. A rigorous analysis of donor/acceptor emission transients, which goes beyond the scope of this paper, would require a quantitative account of the system geometry, as well as of actual exciton distribution in the donor spacing layers.[36,37]

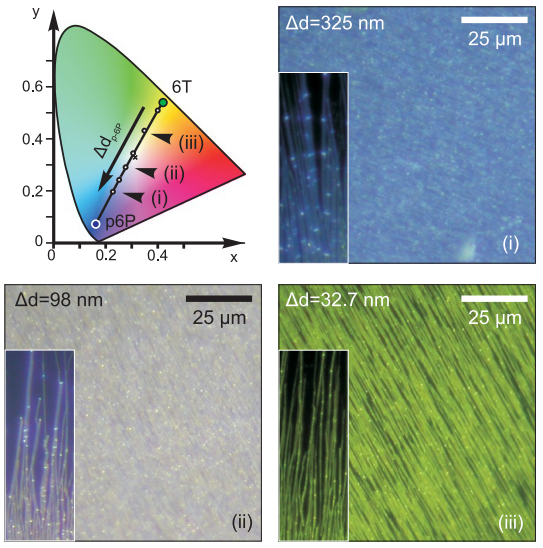

Figure 7. Representation of the nanofibers' emission color by plotting the 1931 Commission Internationale de l'Eclairage (CIE) coordinates for different *p*-6P spacer thicknesses. By decreasing the *p*-6P spacer thickness the contribution of green 6T emission increases, shifting the emission from blue (0.16, 0.07) to yellow-green (0.42, 0.54). Fluorescence images show the emission of light blue (d = 325 nm), white (d = 98 nm), and green (d = 32.7 nm) emitting nanofibers. The fluorescence emission of all fabricated samples indicates a highly homogeneous distribution of 6T and *p*-6P.

As already demonstrated by PL measurements, periodical deposition of *p*-6P and 6T molecules on top of *p*-6P nanofiber templates enables a precise control on the spectral contribution of blue *p*-6P and green 6T emission. In combination with the highly polarized emission of both molecular species such color tuning has certainly high potential for device applications such as organic light emitting diodes (OLED). To discuss nanofibers' fluorescence properties concerning possible device applications it is advantegeous to plot the corresponding 1931 Commission Internationale de l'Eclairage (CIE) coordinates, which is shown in Figure 7. As indicated by a blue (green) dot, the CIE coordinates of pure *p*-6P (sub-ML 6T) emissions are located at (0.16, 0.07) and (0.42, 0.54), respectively. CIE coordinates of fluorescent nanofibers have been calculated from the spectral emissions and are indicated in Figure 7 by white solid circles. In the discussed sample series the number of 6T layers has been kept constant (n = 10), whereas *p*-6P spacer thickness has been varied. Consequently, as indicated by a black solid line, the emission color of *p*-6P/6T nanofibers can be shifted on a straight path from the blue to the yellow-green spectrum simply by decreasing the *p*-6P spacer thickness. Moreover, as indicated by a black cross representing the daylight simulator D65 coordinates (0.31, 0.33), *p*-6P/6T nanofiber emission nicely covers the white spectral range, which is of high significance for possible device applications, for example, white OLEDs. It has to be stated that the demonstrated configuration of *p*-6P and 6T CIE coordinates is highly advantegeous, as white emission can be simply achieved by mixing the spectral emission of only two different molecular species. In general such optical properties are only obtained when blending three to four components.[38] Besides the emission properties, it has to be underlined that the presented *p*-6P/6T nanofibers are fabricated by using only commercially available, frequently investigated, and well understood molecular species. Moreover, nanofibers show macroscopic highly polarized emission within the whole spectral range, which represents a further outstanding property in comparison to recently reported white-light-emitting nanofibers.[38]

SUMMARY AND CONCLUSION

It has been demonstrated by PL measurements that the interfacial, green emitting 6T concentration can be precisely controlled by an alternating deposition of 6T and *p*-6P. In that way, optical emission of the fabricated nanofibers can be spectrally tuned from the yellow-green to blue depending on the chosen periodicity and thickness ratio of *p*-6P/6T layers. Moreover, the formation of 3D-6T crystallites is suppressed when *p*-6P spacers with $\Delta d_{p\text{-}6P} \geq 2.73$ nm are inserted in between the monolayers of 6T molecules. The corresponding 6T concentration at these growth conditions has been estimated to be $\sim$5.55% $\pm$ 0.40% (see Supporting Information). This finding can be explained by the fact that the 6T monolayer is not completely covered by *p*-6P molecules for $\Delta d_{p\text{-}6P} \leq 2.73$ nm which assists the nucleation of 3D-6T crystallites. To substantiate the drawn picture, UPS measurements have been performed indicating a full coverage of the 6T monolayer at a *p*-6P layer thickness of about 1.6 nm. It could be demonstrated that *p*-6P and 6T layers are well separated forming an organic–organic interface. Concerning the homogeneity of nanofibers' height distribution and fluorescence emission, it has been demonstrated by SFM and fluorescence microscopy that the proposed deposition procedure leads to a significant improvement in comparison to that of *p*-6P/6T bilayer structures. Moreover, it has been shown by polarization-dependent photoluminescence experiments that parallel molecular orientation is conserved for all fabricated samples, which represents an essential prerequisite for future device applications. By performing photoluminescence excitation experiments, we demonstrate the occurrence of nonradiative energy transfer between *p*-6P donor and 6T guest molecules, which explains a strongly quenched *p*-6P emission even at low 6T concentrations. Additionally, time-resolved PL shows that acceptor activation dynamics is significantly correlated to the nanofibers' morphology and consistent with the presence of well-separated 6T molecules by *p*-6P spacing layers. The fact that periodical deposition of *p*-6P/6T

molecules yields highly parallel orientated and homogeneously fluorescent nanofibers, whose emission color can be precisely tuned by the chosen *p*-6P/6T periodicity will certainly recommend the chosen approach for future device applications, for example, white OLEDs.

EXPERIMENTAL SECTION

All nanofibers have been fabricated on muscovite mica (001) substrates (SPI - Structure Probe, Inc.) by using hot wall epitaxy (HWE). Muscovite mica is a representative of sheet silicate minerals and provides a layered structure of aluminum silicate sheets weakly bound by layers of potassium ions. Each layer is characterized by a high symmetry direction identified by parallel aligned surface grooves. Between the individual sheets the high symmetry direction alternates by 120° leading to a periodic $\alpha\beta\alpha\beta$ stacking sequence along (001) direction. Immediately after cleaving, the mica substrates were transferred *via* a load lock to the growth chamber containing two separated HWE reactors equipped with *p*-6P (TCI) and 6T (Sigma-Aldrich) source material. The system is operated under high vacuum (HV) conditions with a nominal pressure of 9×10^{-6} mbar. The optimized evaporation temperature for *p*-6P (6T) is given at 240 °C (190 °C) leading to a nominal growth rate of 3.27 ± 0.29 nm/min (4.5 ± 0.35 nm/min). To avoid temperature gradients during growth and to reduce adsorbed species on the surface, the substrate has been preheated at 120 °C for 30 min. The chosen temperature is kept constant during the whole growth procedure. After the growth of the template by depositing *p*-6P for 10 min (~33 nm fiber height) the sample is automatically transferred in HV conditions periodically between the 6T and *p*-6P source oven.

Photoluminescence experiments were performed at room temperature using a He−Cd laser (λ = 325 nm) as an excitation source. The emitted PL radiation was collected and focused into an optical fiber coupled to an Avantes AvaSpec 2048 spectrometer. Epifluorescence images were acquired upon sample illumination by a Hg lamp spectrally narrowed in the 330−360 nm band. For polarization-resolved fluorescence spectroscopy the organic nanofibers were excited over a large area of some hundreds of μm^2 at 375 nm by a frequency-doubled Ti:Sapphire oscillator with 82 MHz repetition frequency. Emission was analyzed by a rotating linear polarizer, wavelength dispersed in a grating spectrometer and detected by a liquid-nitrogen cooled detector.

Time-resolved photoluminescence spectroscopy was performed using a picosecond streak camera coupled to a single grating spectrometer to achieve both temporal and spectral dispersion of the nanofibers' optical emission. Actual time resolution attained in the experiments was approximately 20 ps. Photoluminescence excitation (PLE) spectra were obtained by exciting with a 450 W Xe-lamp monochromated with a double Czerny-Turner GEMINI 180 whose intensity was corrected by using Rhodamine B as a reference. PL was recorded with a SPEX 270 M monochromator equipped with a N_2 cooled charge-coupled device and the spectra were corrected for the instrument response.

Scanning force microscopy (SFM) studies of the deposited nanofibers were performed using a Digital Instruments Dimension 3100 in the tapping mode. The SFM characterization was performed on an area of 10 μm^2 with a SiC tip. The pixel resolution was chosen with 512 × 512 pixels which corresponds to 19.5 nm/pixel. The zero height was corrected by leveling the data to the minimum height of the whole image.

All UPS experiments were carried out at the multichamber ultrahigh vacuum (UHV) endstation SurICat (at beamline PM4) at BESSY II (Berlin, Germany). The highly oriented pyrolythic graphite (HOPG) substrate for the UPS measurements are of ZYA quality and were preheated at 700 K for approximately 15 h. The *p*-6P and 6T molecules were evaporated from a Knudsen cell. During evaporation the HOPG substrates were held at room temperature and the deposition rates were *ca.* 1 Å/min. The film thicknesses given in the text are nominal mass-thickness values determined with a quartz crystal microbalance. Film deposition and UPS measurements were done both in vacuum, and the transfer did not break the vacuum. The UPS spectra were collected with a hemispherical electron energy analyzer (Scienta SES 100) and an excitation energy of 18 eV at 45° emission angle.

Conflict of Interest: The authors declare no competing financial interest.

Acknowledgment. This work has been financially supported by the Austrian Science Fund (FWF), Project Nos. S9706, S9708 and Land Oberösterreich, project "Organische Nanostrukturen". Work in Cagliari was partially funded by MIUR through FIRB projects (Synergy-FIRBRBNE03S7XZ and FIRB-RBAU01N449) and by the European Commission through the Human Potential Programs (RTN Nanomatch, Contract No. MRTN-CT-2006-035884).

Supporting Information Available: Detailed information about sample preperation, structural characterization, SFM investigations, and PL measurements. This material is available free of charge *via* the Internet at http://pubs.acs.org.

REFERENCES AND NOTES

1. Bodnarchuk, M. I.; Kovalenko, M. V.; Heiss, W.; Talapin, D. V. Energetic and Entropic Contributions to Self-Assembly of Binary Nanocrystal Superlattices: Temperature as the Structure-Directing Factor. *J. Am. Chem. Soc.* **2010**, *132*, 11967–11977.
2. Redl, F. X.; Cho, K.-S.; Murray, C. B.; O'Brien, S. Three-Dimensional Binary Superlattices of Magnetic Nanocrystals and Semiconductor Quantum Dots. *Nature* **2003**, *423*, 968–971.
3. Yaghi, O. M.; O'Keeffe, M.; Ockwig, N. W.; Chae, H. K.; Eddaoudi, M.; Kim, J. Reticular Synthesis and the Design of New Materials. *Nature* **2003**, *423*, 705–714.
4. Zhang, S. Fabrication of Novel Biomaterials Through Molecular Self-Assembly. *Nat. Biotechnol.* **2003**, *21*, 1171–1178.
5. Zhang, C.; Zhao, Y. S.; Yao, J. Optical Waveguides at Micro/Nanoscale Based on Functional Small Organic Molecules. *Phys. Chem. Chem. Phys.* **2011**, 10.1039/c0cp02376k.
6. Kim, F. S.; Ren, G.; Jenekhe, S. A. One-Dimensional Nanostructures of π-Conjugated Molecular Systems: Assembly, Properties, and Applications from Photovoltaics, Sensors, and Nanophotonics to Nanoelectronics. *Chem. Mater.* **2011**, *23*, 682–732.
7. Mann, S. Self-Assembly and Transformation of Hybrid Nano-objects and Nanostructures under Equilibrium and Non-equilibrium Conditions. *Nat. Mater.* **2009**, *8*, 781–792.
8. Simbrunner, C.; Nabok, D.; Hernandez-Sosa, G.; Oehzelt, M.; Djuric, T.; Resel, R.; Romaner, L.; Puschnig, P.; Ambrosch-Draxl, C.; Salzmann, I.; *et al.* Epitaxy of Organic Nano-fibers on Sheet Silicates—A Growth Model Based on Experiments and Simulations. *J. Am. Chem. Soc.* **2011**, *133*, 3056–3062.
9. Kankate, L.; Balzer, F.; Niehus, H.; Rubahn, H.-G. Organic Nanofibers from Thiophene Oligomers. *Thin Solid Films* **2009**, *518*, 130–137.
10. Resel, R.; Haber, T.; Lengyel, O.; Sitter, H.; Balzer, F.; Rubahn, H.-G. Origins for Epitaxial Order of Sexiphenyl Crystals on Muscovite (001). *Surf. Interface Anal.* **2009**, *41*, 764–770.
11. Frank, P.; Hlawacek, G.; Lengyel, O.; Satka, A.; Teichert, C.; Resel, R.; Winkler, A. Influence of Surface Temperature and Surface Modifications on the Initial Layer Growth of para-Hexaphenyl on Mica (001). *Surf. Sci.* **2007**, *601*, 2152–2160.

12. Simbrunner, C.; Hernandez-Sosa, G.; Oehzelt, M.; Djuric, T.; Salzmann, I.; Brinkmann, M.; Schwabegger, G.; Watzinger, I.; Sitter, H.; Resel, R. Epitaxial Growth of Sexithiophene on Mica Surfaces. *Phys. Rev. B* **2011**, *83*, 115443.
13. Balzer, F.; Rubahn, H.-G. Growth Control and Optics of Organic Nanoaggregates. *Adv. Funct. Mater.* **2005**, *15*, 17–24.
14. Schiek, M.; Lützen, A.; Koch, R.; Al-Shamery, K.; Balzer, F.; Frese, R.; Rubahn, H.-G. Nanofibers from Functionalized para-Phenylene Molecules. *Appl. Phys. Lett.* **2005**, *86*, 153107.
15. Balzer, F.; Bordo, V. G.; Simonsen, A. C.; Rubahn, H.-G. Isolated Hexaphenyl Nanofibers as Optical Waveguides. *Appl. Phys. Lett.* **2003**, *82*, 10–12.
16. Yanagi, H.; Ohara, T.; Morikawa, T. Self-Waveguided Gain-Narrowing of Blue Light Emission from Epitaxially Oriented *p*-Sexiphenyl Crystals. *Adv. Mater.* **2001**, *13*, 1452–1455.
17. Quochi, F. Random Lasers Based on Organic Epitaxial Nanofibers. *J. Opt.* **2010**, *12*, 024003.
18. Andreev, A.; Quochi, F.; Cordella, F.; Mura, A.; Bongiovanni, G.; Sitter, H. Coherent Random Lasing in the Deep Blue from Self-Assembled Organic Nanofibers. *J. Appl. Phys.* **2006**, *99*, 034305.
19. Quochi, F.; Cordella, F.; Mura, A.; Bongiovanni, G.; Balzer, F.; Rubahn, H.-G. Gain Amplification and Lasing Properties of Individual Organic Nanofibers. *Appl. Phys. Lett.* **2006**, *88*, 041106.
20. Schiek, M.; Balzer, F.; Al-Shamery, K.; Lützen, A.; Rubahn, H.-G. Nanoaggregates from Thiophene/Phenylene Co-oligomers. *J. Phys. Chem. C* **2009**, *113*, 9601–9608.
21. Schiek, M.; Balzer, F.; Al-Shamery, K.; Brewer, J. R.; Lützen, A.; Rubahn, H.-G. Organic Molecular Nanotechnology. *Small* **2008**, *4*, 176–181.
22. Hernandez-Sosa, G.; Simbrunner, C.; Sitter, H. Growth and Optical Properties of α-Sexithiopene Doped para-Sexiphenyl Nanofibers. *Appl. Phys. Lett.* **2009**, *95*, 013306.
23. Simbrunner, C.; Quochi, F.; Hernandez-Sosa, G.; Oehzelt, M.; Resel, R.; Hesser, G.; Arndt, M.; Saba, M.; Mura, A.; Bongiovanni, G.; *et al.* Organic-Organic Heteroepitaxy of Red-, Green-, and Blue-Emitting Nanofibers. *ACS Nano* **2010**, *4*, 6244–6250.
24. Koller, G.; Berkebile, S.; Krenn, J. R.; Netzer, F. P.; Oehzelt, M.; Haber, T.; Resel, R.; Ramsey, M. G. Heteroepitaxy of Organic−Organic Nanostructures. *Nano Lett.* **2006**, *6*, 1207–1212.
25. Oehzelt, M.; Koller, G.; Ivanco, J.; Berkebile, S.; Haber, T.; Resel, R.; Netzer, F. P.; Ramsey, M. G. Organic Heteroepitaxy: *p*-Sexiphenyl on Uniaxially Oriented α-Sexithiophene. *Adv. Mater.* **2006**, *18*, 2466–2470.
26. Balzer, F.; Bordo, V.; Simonsen, A.; Rubahn, H.-G. Optical Waveguiding in Individual Nanometer-Scale Organic Fibers. *Phys. Rev. B* **2003**, *67*, 115408.
27. Ivanco, J.; Haber, T.; Krenn, J.; Netzer, F.; Resel, R.; Ramsey, M. Sexithiophene Films on Ordered and Disordered TiO_2-(110) Surfaces: Electronic, Structural and Morphological Properties. *Surf. Sci.* **2007**, *601*, 178–187.
28. Oehzelt, M.; Grill, L.; Berkebile, S.; Koller, G.; Netzer, F. P.; Ramsey, M. G. The Molecular Orientation of para-Sexiphenyl on Cu (110) and Cu (110)p(2 × 1)O. *Chem.Phys.Chem.* **2007**, *8*, 1707–1712.
29. Horowitz, G.; Bachet, B.; Yassar, A.; Lang, P.; Demanze, F.; Fave, J.-L.; Garnier, F. Growth and Characterization of Sexithiophene Single Crystals. *Chem. Mater.* **1995**, *7*, 1337–1341.
30. Salzmann, I.; Duhm, S.; Heimel, G.; Oehzelt, M.; Kniprath, R.; Johnson, R. L.; Rabe, J. P.; Koch, N. Tuning the Ionization Energy of Organic Semiconductor Films: The Role of Intramolecular Polar Bonds. *J. Am. Chem. Soc.* **2008**, *130*, 12870–12871.
31. Vogel, J.-O.; Salzmann, I.; Duhm, S.; Oehzelt, M.; Rabe, J. P.; Koch, N. Phase-separation and mixing in thin films of co-deposited rodlike conjugated molecules. *J. Mater. Chem.* **2010**, *20*, 4055–4066.
32. Baker, K. N.; Fratini, A. V.; Resch, T.; Knachel, H. C.; Adams, W. W.; Socci, E. P.; Farmer, B. L. Crystal-Structures, Phase-Transitions and Energy Calculations of Poly(*p*-Phenylene) Oligomers. *Polymer* **1993**, *34*, 1571.
33. Becker, R. S.; de Melo, J. S.; Maçanita, A. L.; Elisei, F. Comprehensive Evaluation of the Absorption, Photophysical, Energy Transfer, Structural, and Theoretical Properties of α-Oligothiophenes with One to Seven Rings. *J. Phys. Chem.* **1996**, *100*, 18683–18695.
34. Stampfl, J.; Tasch, S.; Leising, G.; Scherf, U. Quantum Efficiencies of Electroluminescent Poly(para)-phenylenes. *Synth. Met.* **1995**, *71*, 2125.
35. Zojer, E.; Koch, N.; Puschnig, P.; Meghdadi, F.; Niko, A.; Resel, R.; Ambrosch-Draxl, C.; Knupfer, M.; Fink, J.; Bredas, J. L.; *et al.* Structure, Morphology, and Optical Properties of Highly Ordered Films of para-Sexiphenyl. *Phys. Rev. B* **2000**, *61*, 16538–16549.
36. Haynes, D. R.; Tokmakoff, A.; George, S. M. Distance Dependence of Electronic Energy Transfer between Donor and Acceptor Adlayers: *p*-Terphenyl and 9,10-Diphenylanthracene. *J. Chem. Phys.* **1994**, *100*, 1968–1980.
37. Shaw, P. E.; Ruseckas, A.; Samuel, I. D. W. Distance Dependence of Excitation Energy Transfer between Spacer-Separated Conjugated Polymer Films. *Phys. Rev. B* **2008**, *78*, 245201.
38. Giansante, C.; Raggy, G.; Schäfer, C.; Rahma, H.; Kao, M.-T.; Olive, A. G. L.; Guerzo, A. D. White-Light-Emitting Self-Assmebled Nanofibers and Their Evidence by Microspectroscopy of Individual Objects. *J. Am. Chem. Soc.* **2010**, *133*, 316–325.